Control of plasmaspheric dynamics by both convection and sub-auroral polarization stream

J. Goldstein,[1,2] B. R. Sandel,[3] M. R. Hairston,[4] and P. H. Reiff[1]

Received 11 August 2003; revised 12 November 2003; accepted 17 November 2003; published 17 December 2003.

[1] The long-standing hypothesis that plasmaspheric dynamics are described by superposition of corotation and solar-wind-driven sunward convection is tested via direct comparison between plasmasphere observations and simulation output. The observations consist of global plasmasphere images produced by the IMAGE extreme ultraviolet (EUV) imager during plasmasphere erosion on 2 June 2001. The simulation is a plasmapause evolution model driven by a time-varying Volland-Stern (VS) electric potential distribution. On the dawnside and much of the nightside the model matches the EUV plasmapause position to within 0.2–0.5 earth radii (R_E). Near dusk the model plasmapause is about 0.7–1.2 R_E farther out than the EUV plasmapause, suggesting that an improved model should include the duskside flow enhancement known as the sub-auroral polarization stream (SAPS). We demonstrate that including a simplified ad-hoc SAPS potential can correct the model on the duskside. *INDEX TERMS:* 2712 Magnetospheric Physics: Electric fields (2411); 2760 Magnetospheric Physics: Plasma convection; 2768 Magnetospheric Physics: Plasmasphere; *KEYWORDS:* plasmasphere, dynamics, convection. **Citation:** Goldstein, J., B. R. Sandel, M. R. Hairston, and P. H. Reiff, Control of plasmaspheric dynamics by both convection and sub-auroral polarization stream, *Geophys. Res. Lett.*, *30*(24), 2243, doi:10.1029/2003GL018390, 2003.

1. Introduction

[2] The plasmasphere is the cold (1 eV), dense (10^2–10^4 cm^{-3}) torus of plasma occupying the inner magnetosphere out to a boundary known as the plasmapause where the density can drop by 1–2 orders of magnitude in under one Earth radius (R_E). Decades of observation show that the plasmapause radial location moves inward during geomagnetic disturbance periods. To explain this, a long-standing hypothesis is that the dynamics of the plasmasphere are controlled by a superposition of an eastward corotational flow field and a (generally) sunward convection field that is driven by the flow of the solar wind (SW) and interplanetary magnetic field (IMF) past the magnetosphere *Nishida*, [1966]. Enhancements in convection move the corotation/convection boundary inward, causing erosion of the outer plasmasphere as formerly corotating outer flux tubes are carried away in the newly strengthened convection field. A mitigating effect is inner magnetospheric shielding [*Jaggi and Wolf*, 1973], in which coupling between partial ring currents and the finite-conducting ionosphere creates an electric (E) field that counters convection.

[3] Although consistent with zero-order plasmasphere behavior during active times, the simple convective picture ignores some known or suspected complicating effects such as (but not limited to) ionospheric filling, inhomogeneity in ionospheric conductivity, violations of the 'frozen-in-flux' condition, plasmapause interchange instability, large-scale magnetic reconfiguration, and the sub-auroral polarization stream (SAPS) (*Foster and Burke* [2002] and references therein). The SAPS is a strong sunward flow channel observed during active times at the dusk-to-early-morning plasmasheet inner edge, that forms via ionospheric feedback as follows. A gap between the inner edges of the proton and electron plasma sheets generates strong poleward E-fields in the poorly-conducting nightside sub-auroral ionosphere, i.e., mostly radial equatorial E-fields (sunward flow near dusk). On average, ionospheric SAPS are found ~3–5 degrees magnetic latitude (MLAT) below the auroral oval, concentrated most strongly in the dusk/pre-midnight sector [*Foster and Vo*, 2002]. In the equatorial plane the SAPS forms a radially-narrow (≈2 R_E) flow channel bordering/overlapping the duskside and pre-midnight plasmasphere.

[4] The IMAGE satellite extreme ultraviolet (EUV) imager [*Sandel et al.*, 2001] obtains full global plasmasphere images by detecting 30.4 nm light resonantly scattered by plasmaspheric He^+ ions. EUV's lower threshold is 40 e^- cm^{-3} ≈ 4–8 He^+ cm^{-3} [*Goldstein et al.*, 2003b]. EUV images provide a means of evaluating the conventional picture of convection-driven plasmasphere dynamics, in which the plasmapause location is an important and useful indicator of the inner magnetospheric E-field. Using EUV images *Goldstein et al.* [2003a] found that convection dominated the timing of plasmasphere erosion for post-midnight magnetic local time (MLT), but the SAPS flow channel was very likely an important effect near dusk. In this letter we study the global quantitative contributions of shielded convection and SAPS, for an erosion event on 2 June 2001, through direct comparison between EUV images and numerical plasmapause simulation results. We will show that both convection and SAPS play major roles in plasmasphere dynamics during erosion, and SAPS can dominate the duskside when convection is weak.

2. Plasmapause Test Particle Simulation

[5] Plasmasphere dynamics can be modeled by assuming that the plasmapause boundary is comprised of test particles

[1]Department of Physics and Astronomy, Rice University, Houston, Texas, USA.
[2]Now at Space Science and Engineering Division, Southwest Research Institute, San Antonio, Texas, USA.
[3]Lunar and Planetary Laboratory, University of Arizona, Tucson, Arizona, USA.
[4]Center for Space Sciences, University of Texas at Dallas, Richardson, Texas, USA.

0094-8276/03/2003GL018390$05.00

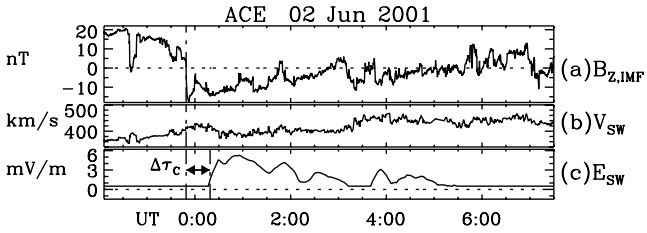

Figure 1. ACE data, 2 June 2001 (a) IMF polarity, (b) solar wind speed, (c) solar wind electric field The southward IMF turning at 23:49 on 1 June triggered plasmaspheric erosion seen by EUV 30 minutes later.

subject to $E \times B$ drift. In a time-varying convection E-field the evolution of the plasmapause is modeled by the changing shape of the curve defined by the aggregate of these test particles, an approach hereinafter called the 'plasmapause test-particle' (PTP) simulation. This approach works best for steep plasmapause radial gradients; an indistinct boundary is obviously not well-represented by a single contour. The convection E-field model chosen to drive the PTP simulations is that of *Volland* [1973] and *Stern* [1975], which can be considered representative of the conventional convection-based picture to be tested in this letter. The Volland-Stern (VS) electric potential function is given by $\Phi_{VS}(r, \varphi) = -A_0 r^{\lambda} \sin \varphi$. The value of λ determines the strength of a primitive shielding effect: $\lambda = 1$ is no shielding (i.e., uniform convection E-field) and $\lambda = 2$ is the shielding value found to best agree with observations [*Volland*, 1973; *Stern*, 1975; *Maynard and Chen*, 1975]. Though an r^{λ} dependence is unrealistic at large r, and oversimplifies the shielding process (e.g., overshielding is ignored), we will show that the suitably normalized VS potential is not an unreasonable representation of inner magnetospheric convection. y trial and error we optimized PTP/EUV dawnside plasmapause agreement with $A_0 = 0.12\ E_{SW} \cdot (6.6\ R_E)^{1-\lambda}$, equivalent to 12 percent of the solar wind E-field applied across the inner magnetosphere inside geosynchronous orbit, not inconsistent with earlier Kp-based normalizations (e.g., *Maynard and Chen* [1975]) that we did not use for the following reasons. (1) EUV images show measurable global changes on time scales faster than the 3-hr Kp cadence. (2) Kp incorporates any disturbance, but we wish to study the effect of solar-wind-driven convection as a distinct process; thus our Φ_{VS} is normalized to E_{SW}. Assuming convection is primarily reconnection-driven during southward IMF, but that there is a finite viscous solar-wind-magnetopause interaction during northward IMF, the solar wind E-field is defined as the product of the solar wind speed and the southward IMF component: $E_{SW} = -V_{SW}B_{Z,\ IMF}$, with the constraint that $E_{SW} \geq 0.5$ mV/m. We assume dipolar magnetic field, a decent approximation in the inner magnetosphere for mild events. In the next section is a direct comparison between the results of this VS-driven PTP simulation and EUV images from 2 June 2001.

3. Plasmasphere Erosion, 2 June 2001

[6] After an extended quiet (Q) period (i.e., no strong southward IMF, presumed ionospheric filling) typical plasmasphere properties seen by IMAGE EUV are: (Q1) gradually decreasing density vs. radius r with no clear plasmapause boundary; (Q2) outlying plasma at large r with density near the EUV lower threshold of 4–8 He^+ cm^{-3}; (Q3) azimuthal density variations and irregular shape. Geomagnetic disturbance typically results in the following plasmasphere erosion (E) scenario: (E1) tenuous outlying nightside plasma disappears; (E2) nightside plasmapause moves to lower r and achieves a steep radial gradient and a relatively smooth azimuthal profile; (E3) dayside plasma moves sunward to form a broad plume. Typically, (E1) occurs early in the erosion. Between 0–6 UT on 2 June 2001, EUV observed erosion that commenced about 00:21 UT, apparently triggered by a southward IMF transition.

[7] Figure 1 summarizes solar wind conditions during the first several hours of 2 June 2001, as seen by ACE [*Stone et al.*, 1998]. The IMF Z-component (1(a)) and SW speed (1(b)) have been propagated to a nominal 10 R_E magnetopause from ACE's 226 R_E (≈55 minutes) upstream location. Following a full day of mostly northward IMF, the IMF turned strongly southward at 23:49 UT on 1 June (the broken vertical line), producing a mild geomagnetic disturbance (Kp 3–5, Dst ≥ -30 nT). About 32 minutes elapsed between the southward IMF turning and the earliest onset of plasmaspheric erosion seen by EUV. This as yet unexplained time delay (hereinafter called $\Delta\tau_C$) between IMF transition and plasmasphere erosion is so far a consistent occurence in EUV data [*Goldstein et al.*, 2003a]. The solar wind E-field in Figure 1(c) (used to drive the PTP simulation; see below) is delayed by $\Delta\tau_C$.

[8] Figure 2 contains EUV observations of the 2 June erosion. In each panel is an EUV image that has been

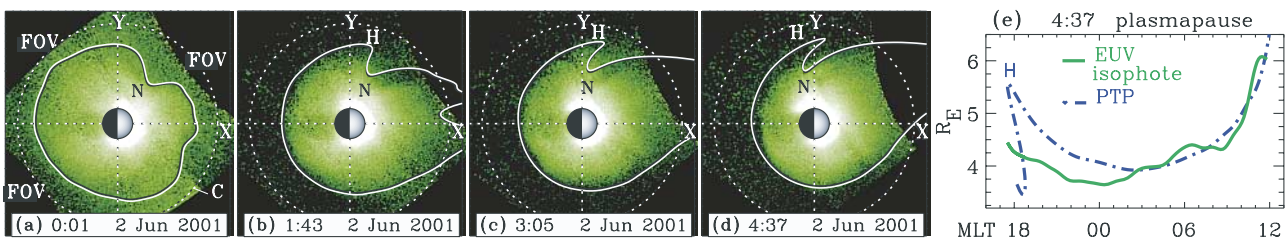

Figure 2. (a)–(d): Four snapshots of the 2 June plasmaspheric erosion Color images show EUV equatorial He^+ abundance 'FOV' = edges of EUV instrument field of view Bright patch 'C' in 2(a) is sunlight contamination, not an isolated plasma blob X, Y axes, and geosynchronous orbit are dotted lines Bold white traces are model curves which mimic plasmapause gradients in EUV images; overall agreement is good except near dusk Panel (e): Plasmapause radius vs MLT at 4:37: EUV (solid/green line) and PTP (broken/blue).

mapped to the magnetic equator [*Goldstein et al.*, 2003b]. The color/intensity is proportional to line-of-sight integrated He^+ column abundance. (In this letter absolute density values are unimportant so no number scale is indicated.) In each panel, the PTP model plasmapause at that time is overlaid on the EUV image as a bold white curve.

[9] The effects of plasmasphere erosion are clear in EUV image sequence 2(a)–2(d). The image in 2(a), taken at 00:01 after a day of quiet conditions, shows typical quiet-time plasmasphere properties (Q1)–(Q3) and a post-noon (∼15 MLT) indentation or 'notch' (labeled 'N'). Figures 2(b), 2(c) and 2(d) depict plasmasphere erosion that follows (E1)–(E3). The EUV nightside plasmapause moves inward ≈2 R_E and becomes well-defined. Sunward plasma motion in 2(a)–2(d) was inferred from increased EUV intensity at larger X in later images. Dayside plasma west of the notch moves sunward to form a broad main plume (between $Y \approx [-5, 3]$ R_E at 1:43 UT). The plasma bulge east of the notch 'N' (near dusk) elongates into a thin duskside plume separated from the main plume by a narrow low-density channel that can be faintly seen as a diffuse strip of reduced EUV intensity extending outward from 'N'. In 2(d) the channel is so narrow as to be almost completely obscured.

[10] The PTP simulation was initialized at 00:01 UT with the bold white curve in Figure 2a, which is an isophote of the EUV image that captures the size and shape of the bulk of the 00:01 UT plasmasphere but ignores the outlying density (hazy, speckled pixels near FOV edge) which disappears early in the erosion. This initial plasmapause was allowed to evolve via finite-differencing (with 1-sec time-steps) under the $\lambda = 2$ Volland-Stern potential driven by E_{SW} of Figure 1(c). The evolution of the simulation is given by the model curves overlaid on the EUV images in Figures 2(b), 2(c) and 2(d). The overall global changes in the EUV images (inward nightside plasmapause motion, sunward dayside plasma surge) are captured by the model. In Figure 2(b) the PTP plasmapause follows the EUV well-defined nightside plasmapause to within 0.2–0.5 R_E. The post-dawn hazy plasma and nightside meso-scale(≈0.1–0.2 R_E) plasmapause 'ripples' are not as well captured by the PTP model's one-contour approachand smooth VS potential. Near dusk, the model overestimates the Y-locations of the notch 'N' and duskside bulge (labeled 'H') by roughly 0.7–1.2 R_E. In 2(c) and 2(d) the EUV dawnside plasmapause continues to be quantitatively well captured by the model. The qualitative duskside disagreement increases in 2(c) and 2(d): the model 'H' bulge stretches sunward (due to convection) into a horn-like shape, but doesn't quite elongate into a plume as happens in EUV images. Figure 2(e) compares the PTP plasmapause radius vs. MLT at 4:37 for EUV and PTP, which agree to within 0.2–0.5 R_E post-midnight, but differ by 0.7–1.2 R_E pre-midnight. This level of agreement is characteristic of the entire event.

[11] The disparity between the model and the EUV images suggests that duskside Volland-Stern flows are too weak. With stronger duskside flows the model horn 'H' should form into a full plume as in the EUV images, and the entire plasmasphere near dusk would be smaller. Stronger duskside flows could also overpower the corotation field, causing the horn and notch to sub-corotate as they do in the EUV images. (e.g., the MLT location of the EUV notch trails that of the model notch in 2(b) and 2(c).) One candidate to strengthen

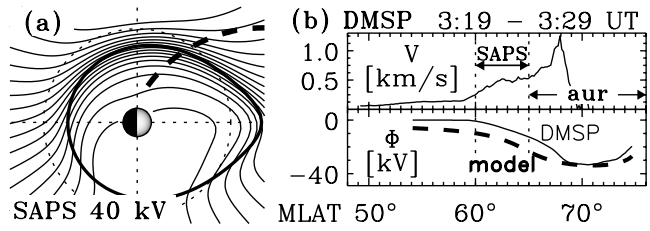

Figure 3. (a) Equatorial ad-hoc SAPS potential; flows are concentrated near dusk along the bold curve (b) DMSP flows (V) and potential (Φ); SAPS and auroral ('aur') regions indicated.

the model flows near dusk is the sub-auroral polarization stream (SAPS) introduced in section 1. Low altitude particle/flow data, recorded by the DMSP satellites on 2 June 2001, indicate a SAPS enhancement at about 1:45 UT, and a strong SAPS event 2:45–4:00 UT [J. Foster, 2003, private communication]. The time interval of the strong SAPS event (2:45–4:00 UT) coincides with the poor afternoon sector performance of the model (2(c)–2(d)). On average, SAPS strength increases gradually across the nightside from dawn (weaker) to dusk (stronger). This qualitative MLT dependence is seen in 2(d) and 2(e) in the size of the gap between the PTP and EUV plasmapause curves, which widens across the nightside from dawn to dusk.

4. Simulation With ad-hoc SAPS Model

[12] Given the duskside disagreement between the model and EUV-observed plasmapause locations we propose that a more accurate inner magnetospheric E-field model can be constructed from superposition of a shielded convection model (e.g., Volland-Stern) and a SAPS model. Although no parametric model of the SAPS E-field is currently available, SAPS statistical properties [*Foster and Vo*, 2002] can in principle be used to construct a SAPS model that can be iteratively improved through comparison with global EUV observations.

[13] To demonstrate the feasibility of this approach in a one-case analysis, we added into the PTP simulation an ad-hoc SAPS model potential (in the equatorial plane):

$$\Phi_S(r,\varphi,t) = -V_S(t)F(r,\varphi)G(\varphi) \tag{1}$$

$$F(r,\varphi) = \frac{1}{2} + \frac{1}{\pi}\tan^{-1}\left[\alpha\{r - R_S(\varphi)\}\right] \tag{2}$$

$$R_S(\varphi)) = R_S^0\left(\frac{1+\beta}{1+\beta\cos(\varphi-\pi)}\right)^{\kappa} \tag{3}$$

$$G(\varphi) = \cos^2\left[\frac{1}{2}(\varphi - \varphi_S)\right]. \tag{4}$$

This Φ_S describes a negative potential drop with a time-dependent magnitude V_S centered at an azimuthally-varying radius R_S, an ellipse-like curve (adapted from *Shue et al.* [1997]) with minimum distance R_S^0 at angle π (i.e., midnight MLT), and eccentricity governed by β and κ. The radial width of the potential drop is controlled by the α parameter in the arctangent of $F(r, \varphi)$, and the strength

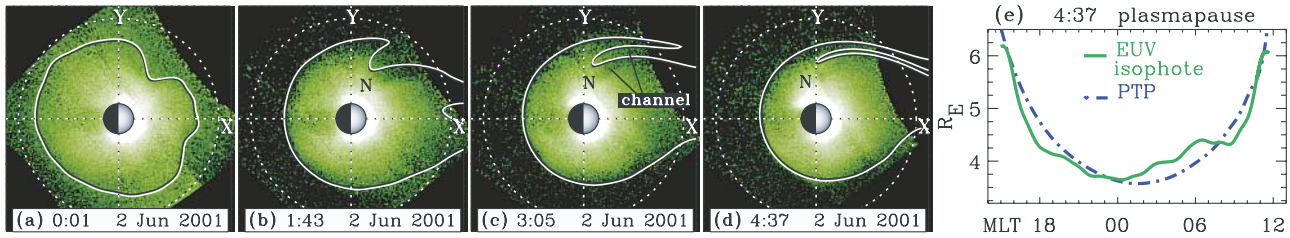

Figure 4. Model results of Figure 2 redone to include SAPS. Compare panels ~4(a)–4(e) to those of Figure 2. With SAPS included, the model's duskside plasmapause is closer to observations, and good dawnside agreement is preserved.

is modulated in local time by $G(\varphi)$, with maximum strength at φ_S. The functional form chosen is simple, analytical, and with suitable parameters mimics average SAPS properties. The SAPS potential with parameters [α, β, κ, R_S^0, φ_S] = [0.9, 0.97, 0.14, 4.9 R_E, $\pi/2$], and magnitude V_S = 40 kV is depicted in Figure 3a. The V_S potential drop along $R_S(\varphi)$ (bold curve), is concentrated at dusk ($\varphi = \pi/2$). The simple $\cos^2$ dependence in $G(\varphi)$ gives unrealistically large SAPS flows in the pre-dusk sector, but the large SAPS radius R_S in that sector minimizes the effect on the plasmasphere. We chose $V_S(t)$ to very crudely represent the DMSP-deduced SAPS time profile mentioned at the end of the previous section: $V_S(t) = 40$ kV [0.3 exp{$-(t - 1.75)^2/(1$ UT hr)^2} + exp{$-(t - 3.38)^2/(1$ UT hr)^2}]. Our Φ_S is merely an interpretation of *Foster and Vo* [2002] that optimizes PTP/EUV agreement, but nonetheless agrees fairly well with available observations. Figure 3(b) shows DMSP F13 data from 3:19–3:27, during peak SAPS activity (and minimal convection). The top panel shows the sunward flow speed V vs. MLAT (minus co-rotation) along the F13 orbit. Subauroral (60–65° MLAT) 300–500 m/s flows are SAPS. The bottom panel plots F13 Φ [kV] (solid line) relative to $\Phi(58°)$. The thick dashed line is the model Φ_S at dipole L values along F13's orbit (dashed line in 3(a)). Aside from a ~9 kV offset, the model's 13 kV subauroral potential drop is quite close to DMSP's (12 kV).

[14] In Figure 4 are the results of incorporating Φ_S into the 2 June PTP simulation; model plasmapause curves (bold lines) are overlaid on EUV images (color scale) in the same format as Figure 2. The inclusion of SAPS yields much better duskside agreement, and because SAPS flows are localized near dusk/pre-midnight, preserves good dawnside agreement. Note that with SAPS the model horn feature of 2 June 2001 evolves correctly into a thin duskside plume separated from the main dayside plume by a thin channel. SAPS dominate the duskside region during weak convection. At 3:21 the 18 MLT subauroral $\Delta\Phi_S$ potential drop is 22 kV ($E \sim 1$–1.5 mV/m), but with E_{SW} = 0.5 mV/m $\Delta\Phi_{VS}$ is only 2 kV ($E < 0.1$ mV/m).

[15] The ad-hoc SAPS potential Φ_S (designed for this one case study only) is not accurate in a detailed sense; e.g., the improved model's afternoon-sector notch ('N' in Figure 4) and low-density channel still lie eastward of the true location in the EUV images. However, improved model performance on the duskside clearly demonstrates that simple shielded convection is quantitatively inadequate in events where SAPS are observed, and that SAPS and convection must be treated as two distinct processes. The SAPS flow region can play a major role in determining the location of the duskside plasmapause and can create additional thin duskside plumes.

5. Concluding Remarks

[16] For the 2 June 2001 plasmasphere erosion witnessed by the EUV imager, the Volland-Stern (VS) electric potential was employed in a solar-wind-driven, time-dependent plasmapause test particle (PTP) simulation. In this letter the VS potential represents the traditional convection picture, which holds that the main influences that govern plasmasphere evolution are convection and shielding (plus corotation). IMAGE EUV global plasmasphere images allowed us to test this picture on a global scale using the plasmapause as an E-field diagnostic. In this event we found that on the dawnside and much of the nightside, the time-dependent global plasmapause shape and location can be well-described (to within a few tenths of an R_E) by a convection-based model. However, we have demonstrated that the observed duskside plasmapause evolution may not be captured by convection alone, and that the addition of a simple ad-hoc representation of the sub-auroral polarization stream (SAPS) can in principle account for this discrepancy. Our result indicates the need to consider coupling/feedback between magnetosphere and ionosphere in global inner magnetospheric dynamics as a process distinct from solar-wind-driven convection. Future development of this approach should involve (1) creation of a general-use SAPS model whose spatial form and intensity are parameterized by geomagnetic activity level according to *Foster and Vo* [2002], (2) simulation of the entire plasma distribution, not just the plasmapause shape, and (3) studying the importance of additional effects such as more spatially structured convection, more realistic shielding and magnetic field, ionospheric filling, and interchange instability.

[17] **Acknowledgments.** We thank N. Ness, C. Smith, D. McComas, the ACE science center for SW/IMF data; the IMAGE program under NASA contract NAS5-96020 (Sandel, Reiff, Goldstein); NASA SEC GI grant NAG5-12787 (Goldstein); NSF ATM-0101118 and NASA NAG5-9297 (Hairston).

References

Foster, J. C., and W. J. Burke, SAPS: A new categorization for sub-auroral electric fields, *Eos Trans AGU*, *83*(36), 393–394, 2002.

Foster, J. C., and H. B. Vo, Average characteristics and activity dependence of the subauroral polarization stream, *J. Geophys. Res.*, *107*(A12), 1475, doi:10.1029/2002JA009409, 2002.

Goldstein, J., B. R. Sandel, W. T. Forrester, and P. H. Reiff, IMF-driven plasmasphere erosion of 10 July 2000, *Geophys. Res. Lett.*, *30*(3), 1146, doi:10.1029/2002GL016478, 2003a.

Goldstein, J., M. Spasojević, P. H. Reiff, B. R. Sandel, W. T. Forrester, D. L. Gallagher, and B. W. Reinisch, Identifying the plasmapause in IMAGE EUV data using IMAGE RPI in situ steep density gradients, *J. Geophys. Res.*, *108*(A4), 1147, doi:10.1029/2002JA009475, 2003b.

Jaggi, R. K., and R. A. Wolf, Self-consistent calculation of the motion of a sheet of ions in the magnetosphere, *J. Geophys. Res.*, *78*(16), 2852–2866, 1973.

Maynard, N. C., and A. J. Chen, Isolated cold plasma regions: Observations and their relation to possible production mechanisms, *J. Geophys. Res.*, *80*, 1009–1013, 1975.

Nishida, A., Formation of plasmapause, or magnetospheric plasma knee, by the combined action of magnetospheric convection and plasma escape from the tail, *J. Geophys. Res.*, *71*, 5669–5679, 1966.

Sandel, B. R., R. A. King, W. T. Forrester, D. L. Gallagher, A. L. Broadfoot, and C. C. Curtis, Initial results from the IMAGE extreme ultraviolet imager, *Geophys. Res. Lett.*, *28*(8), 1439–1442, 2001.

Shue, J.-H., J. K. Chao, H. C. Fu, C. T. Russell, P. Song, K. K. Khurana, and H. J. Singer, A new functional form to study the solar wind control of the magnetopause size and shape, *J. Geophys. Res.*, *102*(A5), 9497–9511, 1997.

Stern, D. P., The motion of a proton in the equatorial magnetosphere, *J. Geophys. Res.*, *80*, 595, 1975.

Stone, E. C., A. M. Frandsen, R. A. Mewaldt, E. R. Christian, D. Margolies, J. F. Ormes, and F. Snow, The Advanced Composition Explorer, *Space Sci. Rev.*, *86*, 1, 1998.

Volland, H., A semiempirical model of large-scale magnetospheric electric fields, *J. Geophys. Res.*, *78*, 171–180, 1973.

J. Goldstein, SwRI, 6220 Culebra Rd, San Antonio, TX 78228, USA. (jgoldstein@swri.edu)

B. R. Sandel, LPL, University of Arizona, Tucson, AZ 85721, USA.

P. H. Reiff, Rice University, MS108, Houston, TX 77005, USA.

M. R. Hairston, UTD, P.O. Box 830688 FO22, Richardson, TX 75083, USA.